Carrier Concentration Analysis in 1.2 kV SiC Schottky Diodes Under Current Crowding

F. Bonet, O. Aviñó-Salvadó, *Member, IEEE*, M. Vellvehi, X. Jordà, P. Godignon, and X. Perpiñà

***Abstract*— Die-level current crowding phenomena are analyzed at the microsecond timescale with an internal IR-Laser Deflection set-up. To this end, the 4H-SiC plasma-optical coefficient for the refractive index is reported for the first time. A SiC Schottky diode with an edge termination based on a junction termination extension is used as a test vehicle. Under biasing conditions, the edge termination starts a local bipolar conduction along the device active area perimeter, leading to current crowding effects. Using refractive index measurements, a depth-resolved carrier profile is extracted and assessed using both, simulation and Free Carrier Absorption measurements.**

***Index Terms*— IIR-LD, current crowding, SiC Schottky diode, plasma-optical coefficient, filamentary conduction.**

I. Introduction

CURRENT crowding is a non-homogeneous conduction mechanism in the power devices drift region. It usually occurs at local areas with a lowered resistance or a high concentrated electric field strength, compromising the device performance, reliability and ruggedness [1]–[3]. This effect is studied and partially avoided by design using physics-based simulations [4], [5]. This entails limitations to quantitatively predict such an effect for wide bandgap (WBG) power devices and/or its geometrical study (3D effects), as some of these parameters or models have not been properly assessed [6], [7]. To this end, measuring carrier density under current crowding is crucial. Based on carrier power absorption of a laser beam, the Free-Carrier Absorption (FCA, mainstream technique) may be used [8]–[11], but with drawbacks. In WBG vertical devices, its accuracy is limited by, not only the lack of specific calibration approaches, but also the device slicing and similar thickness of its drift region to the beam diameter [10]–[12], as they distort the actual carrier density and detected laser power [13].

In this work, Internal Infrared Laser Deflection (IIR-LD) technique is applied to a whole power device [8], [9] to extract for the first time, carrier density profiles under current crowding. Thereby, all prior drawbacks are overcome, as the beam power and sample preparation do not affect IIR-LD results [14]. Besides, calibration approaches for IIR-LD and FCA are presented. Thus, the IIR-LD suitability is proved using a 1.2 kV SiC Schottky diode, physics-based Technology Computer Aided Design (TCAD) simulations and FCA results.

Manuscript received April 2, 2022; revised April 16, 2022 and April 22, 2022; accepted April 26, 2022. Date of publication April 28, 2022; date of current version May 24, 2022. This work was supported in part by the Agencia Estatal de Investigación (AEI) under Contract RTI2018-098392-B-100, Contract PCI2020-112028, and Contract FJC2019-040660-I and in part by the EU H2020 iRel40 Project, under Contract H2020-662133, in the framework of the Ph.D. Program in Physics of the Universitat Autònoma de Barcelona (UAB). The review of this letter was arranged by Editor B. G. Malm. *(Corresponding author: F. Bonet.)*

The authors are with the Institut de Microelectrònica de Barcelona-Centre Nacional de Microelectrònica (IMB-CNM, CSIC), Esfera UAB, Barcelona, 08193 Bellaterra, Spain (e-mail: ferran.bonet@imb-cnm.csic.es).

Color versions of one or more figures in this letter are available at https://doi.org/10.1109/LED.2022.3171112.

Digital Object Identifier 10.1109/LED.2022.3171112

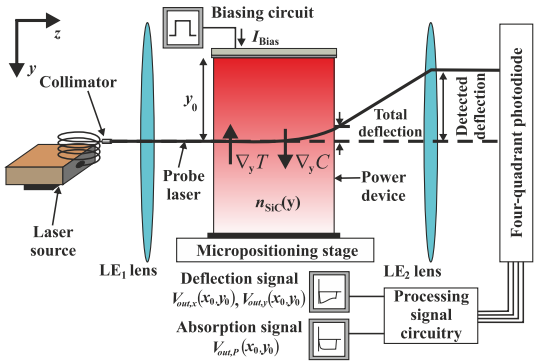

Fig. 1. IIR-LD probing at a given depth y_0 and lateral position x_0, with all the involved physical effects [9].

II. Experimental Set-Up and Test Vehicle

Fig. 1 outlines the operation principle of IIR-LD and FCA, together with their common experimental set-up [9]. At a given depth y_0 and lateral position x_0, an 1.3 µm-laser beam passes through a power device die, perpendicularly striking on its two opposite lateral sidewalls. When the device is turned-on, free-carriers are injected into its drift region and self-heating starts, observing several effects on the probe beam. On one hand, gradients of free-carrier density ($\vec{\nabla}C$) and temperature ($\vec{\nabla}T$) appear, inducing a refractive index gradient $\vec{\nabla}n$ [6] as

$$\vec{\nabla}n(x_0, y_0) = \frac{\partial n}{\partial C}\vec{\nabla}C(x_0, y_0) + \frac{\partial n}{\partial T}\vec{\nabla}T(x_0, y_0) \quad (1)$$

where $\frac{\partial n}{\partial C}$ and $\frac{\partial n}{\partial T}$ are respectively the plasma and thermo-optical coefficients for n. As a result, the beam diverts as depicted in Fig. 1. Thanks to a four quadrant photodiode, two signals are provided depending on the deflection direction, i.e., $V_{out,y}(x_0, y_0)$ and $V_{out,x}(x_0, y_0)$. They relate with the x and y components of $\vec{\nabla}n(x_0, y_0)$ as $\nabla_i n(x_0, y_0) = \xi V_{out,i}(x_0, y_0)$; where i refers to the x or y direction and ξ is a set-up constant. On the other hand, free-carriers partially absorb IR-radiation. Thus, C at y_0 and x_0 is inferred by measuring the laser power signal ($V_{out,P}(x_0, y_0)$) after traversing the die, i.e.:

$$C(x_0, y_0) = \frac{\Delta_P(x_0, y_0)}{L_1}\left(\frac{\partial \alpha}{\partial C}\right)^{-1} \quad (2)$$

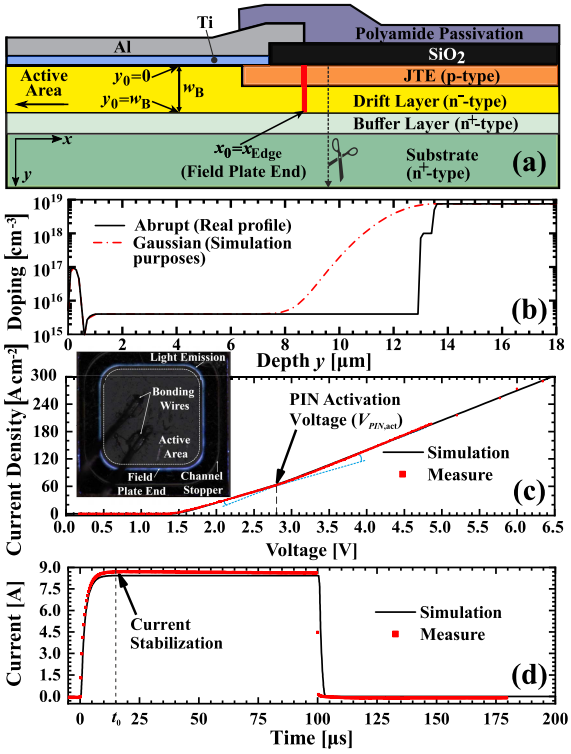

Fig. 2. (a) JTE edge termination structure, highlighting $x_0 = x_{Edge}$ and the doping profile cut. (b) Doping profile used in the simulations. Experimental and simulation results comparison at room temperature for: (c) static I-V characteristic (normalized to device total area) and (d) I_{Bias} waveform. Fig. 2c insert: blue electroluminescence at 3.3 V and 86 A/cm^2 by JTE bipolar activation.

where L_1 and $\frac{\partial \alpha}{\partial C}$ are the laser-device interaction length and the plasma-optical coefficient for the absorption coefficient α, respectively. $\Delta_P(x_0, y_0)$ corresponds to

$$\Delta_P(x_0, y_0) = \ln\left(\frac{V_{out,P_0}(x_0, y_0)}{V_{out,P}(x_0, y_0)}\right). \tag{3}$$

$V_{out,P_0}(x_0, y_0)$ is $V_{out,P}(x_0, y_0)$ before turning the device on. In comparison to FCA, IIR-LD is more robust to laser power fluctuations, as deflections are sensed by normalizing the signals to the detected total power [14]. Moreover, when the beam dimensions are similar to the drift region thickness, the IIR-LD depth-resolved capability comes from the laser light distribution. This profile corresponds to all multiple rays composing the beam [15]. Therefore, the vertical micropositioning stage fixes the IIR-LD depth resolution.

To show the potential of IIR-LD for current crowding analysis, a 1.2 kV Schottky SiC diode (1.6 mm×1.6 mm active area) with an edge termination based on Junction Termination Extension (JTE) is used as a test vehicle. Figs. 2a and 2b represent a section of the test device and its doping profile, respectively. Fig. 2a presents a 13 µm-thick drift region with a n-type doping level of 4×10^{15} cm^{-3}, a 0.5 µm-thick n-type buffer layer of 10^{18} cm^{-3} and a n$^+$-type substrate with 7.5×10^{18} cm^{-3} (see Abrupt in Fig. 2b). The Schottky contact is implemented with Titanium. The p-type JTE consists of a multiple Aluminum ion implantation at 300 °C with a dose of 1.1×10^{13} cm^{-2} and post annealing at 1600 °C during 30 mins. (doping peak of 9.9×10^{16} cm^{-3} measured by SIMS), using a SiO_2 layer as a field plate. Prior to its measurement, this device is properly prepared. First, the lateral

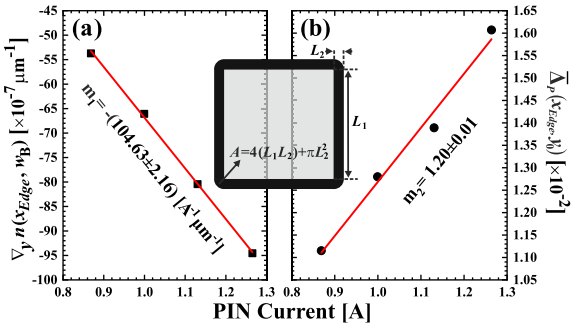

Fig. 3. Calibration results on 4H-SiC for both techniques: (a) IIR-LD and (b) FCA. *A* definition used in (4) and (6).

walls interacting with the laser beam are polished to enhance its transmissivity until reaching an optical grade (RMS surface roughness below 60 nm). After that, the die is soldered on a power substrate and their contacts established with Aluminium bonding wires. Thereby, its handling, support, and biasing are facilitated. To induce current crowding conduction in the test vehicle, the device is placed at room temperature on a heat sink and set under short pulsed current I_{Bias} ranging from 215 to 330A/cm^2 (100 µs) [9]. All the measurements are conducted with a die-averaged beam diameter of 15.5 µm (minimum 8 µm) below the field plate edge end ($x_0 = x_{Edge}$, see Fig. 2a).

TCAD simulations [18] are performed to assess the experiments with different physical models and doping profiles (see Fig. 2b). Firstly, simulations are carried out for the abrupt doping profile under the conditions of incomplete ionization (II) of the dopants [18] usually present at room temperatures in WBG semiconductors. From an electrical viewpoint, they are properly set up to match the test vehicle behavior. Figs. 2c and 2d compare at room temperature, the simulation results with the experimental static I-V characteristics and dynamic response to the I_{Bias} pulse, respectively, observing in both cases an excellent agreement. Moreover, the simulation results actually evidence bipolar injection in the JTE area for the voltage drop reached under I_{Bias}. This can be observed in Fig. 2c, where for voltages higher than $V_{PIN,act}$ =2.8 V, the slope slightly changes (see dashed lines in Fig 2c). The inset of Fig 2c also supports the JTE bipolar injection at voltage values higher than $V_{PIN,act}$: at 86 A/cm^2 and 3.3 V, blue electroluminescence occurs at the end of the field plate [16], [17]. Secondly, for further analysis, a Gaussian transition between the drift and the high doped layers in a span of 5 µm is also taken into account (see Fig. 2b) considering both complete and incomplete ionization. Thus, a set of $C(x = x_{Edge}, y)$ profiles is extracted to discuss experimental results.

III. Results and Discussion

A. IIR-LD and FCA Measurements Calibration

To acquire the contribution of only $\vec{\nabla}C$ (i.e., $\vec{\nabla}T \approx 0$), deflection measurements at the time instant t_0 where I_{Bias} stabilizes to a current value I_0 (i.e., t_0 =15.6 µs) are used, as highlighted in Fig. 2c. Currently, no experimental value of $\frac{\partial n}{\partial C}$ for 4H-SiC is reported. Thus, to be able to derive C from IIR-LD results and as a novelty, $\frac{\partial n}{\partial C}$ is extracted using

$$\nabla_y n(x_{Edge}, w_B) = \frac{\partial n}{\partial C}\frac{\eta I_0}{qAD_n} \tag{4}$$

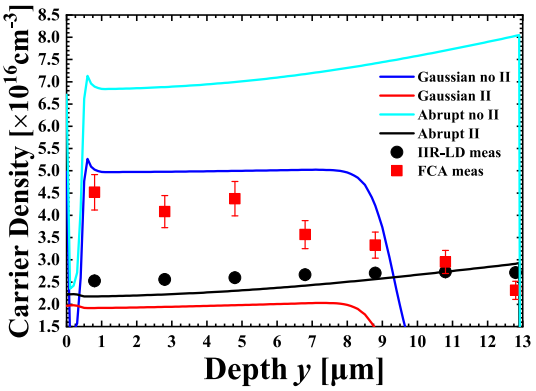

Fig. 4. Comparison of carrier profiles at $x_0 = x_{Edge}$ between experiments and various simulated doping profiles for $I_0 = 8.7A$.

where w_B is the drift zone thickness, q is the electron elemental charge and D_n is the electron diffusion constant in 4H-SiC. Besides, η is the I_0 fraction diverted through the parasitic PIN, and A is the area traversed by the PIN current (i.e., ηI_0) at $y = w_B$ (see inset Fig. 3). η has been inferred by fitting simulations results to experiments ($\eta = 0.115$), as Fig. 2b shows. Eq. (4) is derived from the condition of hole current equal to zero at the device's drift zone end [19]. To calculate A, the shape and dimensions seen in the insert of Fig. 3 are used. L_1 is measured directly on the sample by using an optical microscope. L_2 is extracted from the simulations as the distance between the 1^{st} and 99^{th} percentile of carrier concentration in the x-axis at $y_0 = w_B$. Using (4) and performing a linear fitting of $\nabla_y n$ versus the PIN current (i.e., ηI_0), whose slope is

$$m_1 = \frac{\partial n}{\partial C}\frac{10^7}{qAD_n}, \tag{5}$$

the plasma-optical coefficient for n is calculated. The linear fitting is presented in Fig. 3a, yielding for a wavelength of 1.3 μm, $\frac{\partial n}{\partial C} = -(3.21 \pm 0.07) \times 10^{-21}\ cm^3$.

For the FCA measurements, $\frac{\partial \alpha}{\partial C}$ is required. For consistency, $V_{out,P}(x_0, y_0)$ is acquired at t_0. Considering the mean C in the drift region of a PIN diode [19], i.e., the mean $\Delta_P(x_{Edge}, y_0)$ along y $\left(\overline{\Delta}_P(x_{Edge}, y_0)\right)$, $\frac{\partial \alpha}{\partial C}$ can be extracted using

$$\overline{\Delta}_P(x_{Edge}, y_0) = 2\frac{\eta I_0}{A}\frac{L_1 \tau_{HL}}{q w_B}\frac{\partial \alpha}{\partial C} \tag{6}$$

where τ_{HL} is the bipolar carrier lifetime. Here, this value is calculated using Open-Circuit Voltage Decay (OCVD) measurements [20], [21], obtaining a result of $\tau_{HL} = 247 \pm 5$ ns in accordance with [20]. After this step, $\frac{\partial \alpha}{\partial C} = (2.87 \pm 0.29) \times 10^{-18}\ cm^2$ is finally derived. Fig. 3b depicts the linear fitting, whose slope m_2 relates with $\frac{\partial \alpha}{\partial C}$ as

$$m_2 = \frac{\partial \alpha}{\partial C}\frac{2L_1 \tau_{HL} 10^2}{Aq w_B}. \tag{7}$$

In [22], $\frac{\partial \alpha}{\partial C} = 4.45 \times 10^{-18}$ cm^2 is reported. This disparity may be due to the approach used in [22]: light pumping the free-carriers and probing them with a polarized laser.

B. Free Carrier Concentration Analysis

As a summary, Fig. 4 compares at $x_0 = x_{Edge}$, the C profiles simulated and measured in the drift region. The solid lines correspond to simulation results. They are labeled in accordance with its doping profile (Gaussian or Abrupt) and its dopant ionization state: "no II" for complete ionization and "II" for incomplete ionization. The IIR-LD and the simulation results agree when the abrupt doping transition at $y_0 = w_B$ and II model are considered ("Abrupt II"). However, the experimental results present less variation with depth than the abrupt II one. This evidences a possible lower injection from the n^+ layer at $y_0 = w_B$. This behavior may be ascribed to a less abrupt transition, as a Gaussian profile with and without assuming II is considered in Fig. 4. Examining in Fig. 4 the simulated profiles under such assumptions, the "Gaussian no II" and "Abrupt no II" highly differ from the other two. This, paired with the fact that II occurs in 4H-SiC, is enough to rule out these simulated results as an inaccurate. The "Gaussian II" one produces a profile closer in shape to the IIR-LD results, but with lower C values and starting to decay at 8 µm. This denotes a transition between the n^- and n^+ layers beginning at a lower depth than in the "Abrupt II" one.

Moreover, in a device like the studied here, diffusion of the dopants as high as to create a Gaussian profile is not expected. Therefore, the "abrupt II" results best describe the experiments. The slight mismatch between the measured and abrupt simulation profiles ($\leq$12%) can be linked to a lower JTE injection efficiency predicted by the simulations.

The C profile measured with FCA is also presented in Fig. 4. Even though the results are of the same order of magnitude than the simulations and IIR-LD measurements, the shape is very different, rapidly decreasing with depth. This shape can be attributed to be inspecting drift regions with thicknesses comparable to the probing-laser beam diameter. Thus, the FCA approach is not suitable for this application. Nevertheless, these results serve to validate the IIR-LD measurements, as they show light absorption by the parasitic PIN bipolar carrier injection. It can also be observed that the IIR-LD technique provides a higher accuracy when measuring current crowding phenomena in thin drift regions.

IV. Conclusion

For the first time, current crowding phenomena have been investigated along the JTE-edge termination of a functional 1.2 kV SiC Schottky diode using the IIR-LD technique. Besides, to extract the carrier profile, the 4H-SiC plasma-optical coefficient has also been inferred with an innovative method.

To assess the IIR-LD results, they have been compared with FCA measurements, calibrated with a novel physics-based approach, and TCAD simulations. In contrast to FCA, IIR-LD findings are less affected when the drift region thickness is of the same order of magnitude than the beam diameter, also exhibiting a much better accuracy thanks to the beam intensity distribution and their independence from the laser total power. Besides, IIR-LD and abrupt-doping simulation results excellently agree. The observed differences ($\leq$12%) suggest that a lower carrier efficiency injection in the JTE junction is predicted by the simulations.

As another application, the approach proposed for the plasma-optical coefficient determination may be exploited for using SiC as a material for optoelectronics or power devices simulation purposes, for instance to better calculate heat dissipation under bipolar injection.

REFERENCES

[1] B. Wang, J. Cai, X. Du, and L. Zhou, "Review of power semiconductor device reliability for power converters," *CPSS Trans. Power Electron. Appl.*, vol. 2, no. 2, pp. 101–117, Jun. 2017, doi: 10.24295/CPSSTPEA.2017.00011.

[2] T.-Y. Hung, L.-L. Liao, C. C. Wang, W. H. Chi, and K.-N. Chiang, "Life prediction of high-cycle fatigue in aluminum bonding wires under power cycling test," *IEEE Trans. Device Mater. Rel.*, vol. 14, no. 1, pp. 484–492, Mar. 2014, doi: 10.1109/TDMR.2013.2288703.

[3] E. Özkol, S. Hartmann, and G. Pâques, "Improving the power cycling performance of the emitter contact of IGBT modules: Implementation and evaluation of stitch bond layouts," *Microelectron. Reliab.*, vol. 54, no. 12, pp. 2796–2800, Dec. 2014, doi: 10.1016/j.microrel.2014.08.015.

[4] S. Palanisamy, J. Kowalsky, J. Lutz, T. Basler, R. Rupp, and J. Moazzami-Fallah, "Repetitive surge current test of SiC MPS diode with load in bipolar regime," in *Proc. IEEE 30th Int. Symp. Power Semiconductor Devices ICs (ISPSD)*, May 2018, pp. 367–370, doi: 10.1109/ISPSD.2018.8393679.

[5] E. A. Jones, F. F. Wang, and D. Costinett, "Review of commercial GaN power devices and GaN-based converter design challenges," *IEEE J. Emerg. Sel. Topics Power Electron.*, vol. 4, no. 3, pp. 707–719, Sep. 2016, doi: 10.1109/JESTPE.2016.2582685.

[6] X. Perpina, I. Cortes, J. Urresti-Ibanez, X. Jorda, and J. Rebollo, "Layout role in failure physics of IGBTs under overloading clamped inductive turnoff," *IEEE Trans. Electron Devices*, vol. 60, no. 2, pp. 598–605, Feb. 2013, doi: 10.1109/TED.2012.2228271.

[7] R. Baburske, F. J. Niedernostheide, J. Lutz, H. J. Schulze, E. Falck, and J. G. Bauer, "Cathode-side current filaments in high-voltage power diodes beyond the SOA limit," *IEEE Trans. Electron Dev.*, vol. 60, no. 7, pp. 2231–2308, Aug. 2013, doi: 10.1109/TED.2013.2264839.

[8] X. Perpina, X. Jorda, M. Vellvehi, M. Mermet-Guyennet, J. Millan, and N. Mestres, "Depth-resolved temperature measurements on power devices under transient conditions," in *Proc. 19th Int. Symp. Power Semiconductor Devices IC's*, Jeju, South Korea, May 2007, pp. 33–36, doi: 10.1109/ISPSD.2007.4294925.

[9] X. Perpiñà, X. Jordà, N. Mestres, M. Vellvehi, P. Godignon, J. Millán, and H. V. Kiedrowski, "Internal infrared laser deflection system: A tool for power device characterization," *Meas. Sci. Technol.*, vol. 15, no. 5, pp. 1011–1018, Apr. 2004, doi: 10.1088/0957-0233/15/5/034.

[10] D. Werber, M. Aigner, D. Denoth, F. Wittmann, and G. Wachutka, "Investigation of the internal carrier distribution in 4H-SiC pin-diodes by laser absorption experiments," *Mater. Sci. Forum*, vols. 600–603, pp. 493–496, Sep. 2009, doi: 10.4028/www.scientific.net/MSF.600-603.493.

[11] D. Werber and G. Wachutka, "Time-resolved investigation on the internal carrier distribution in 4 H-SiC pin diodes by laser absorption experiments," in *Proc. 9th Int. Seminar Power Semiconductors (ISPS)*, Prague, Czech Republic, 2008, pp. 41–47, doi: 10.1049/ic:20080181.

[12] D. Werber and G. Wachutka, "Interpretation of laser absorption measurements on 4H-SiC bipolar diodes by numerical simulation," in *Proc. SISPAD*, 2008, pp. 531–534, doi: 10.1109/SISPAD.2008.4648244.

[13] X. Perpiñà, X. Jordà, M. Vellvehi, J. Vobecky, and N. Mestres, "Analysis of excess carrier concentration control in fast-recovery high power bipolar diodes at low current densities," *J. Electrochem. Soc.*, vol. 157, no. 7, p. H711, May 2010, doi: 10.1149/1.3421974.

[14] X. Perpiñà, X. Jordà, M. Vellvehi, and J. Millán, "Development of an analog processing circuit for IR-radiation power and noncontact position measurements," *Rev. Sci. Instrum.*, vol. 76, no. 2, Jan. 2005, Art. no. 025106, doi: /10.1063/1.1851472.

[15] E. L. Lasalle, F. Lepoutre, and J. P. Roger, "Probe beam size effects in photothermal deflection experiments," *J. Appl. Phys.*, vol. 64, no. 1, pp. 1–5, Jul. 1988, doi: 10.1063/1.341463.

[16] H. Luo, J. Mao, C. Li, F. Iannuzzo, W. Li, and X. He, "Online junction temperature and current simultaneous extraction for SiC MOSFETs with electroluminescence effect," *IEEE Trans. Power Electron.*, vol. 37, no. 1, pp. 21–25, Jan. 2022, doi: 10.1109/TPEL.2021.3094924.

[17] L. Ceccarelli, H. Luo, and F. Iannuzzo, "Investigating SiC MOSFET body diode's light emission as temperature-sensitive electrical parameter," *Microelectron. Rel.*, vols. 88–90, pp. 627–630, Sep. 2018, doi: 10.1016/j.microrel.2018.07.027.

[18] *Sentaurus TCAD Tools Suite*, Synopsys, Mountain View, CA, USA, 2013.

[19] J. Lutz, H. Schlangenotto, U. Scheuermann, and R. De Doncker, *Semiconductor Power Devices: Physics, Characteristics, Reliability*. Berlin, Germany: Springer, 2011, doi: 10.1007/978-3-642-11125-9.

[20] G. Sozzi, M. Puzzanghera, G. Chiorboli, and R. Nipoti, "OCVD lifetime measurements on 4H-SiC bipolar planar diodes: Dependences on carrier injection and diode area," *IEEE Trans. Electron Devices*, vol. 64, no. 6, pp. 2572–2578, Jun. 2017, doi: 10.1109/TED.2017.2691280.

[21] J. Vobecký, P. Hazdra, and V. Záhlava, "Open circuit voltage decay lifetime of ion irradiated devices," *Microelec. J.*, vol. 30, no. 6, pp. 513–520, Jun. 1999, doi: 10.1016/S0026-2692(98)00173-6.

[22] V. Grivickas, A. Galeckas, P. Grivickas, and J. Linnros, "Determination of the polarization dependence of the free-carrier-absorption in 4H-SiC at high-level photoinjection," in *Materials Science Forum*, vol. 338. Cham, Switzerland: Trans Tech Publications, May 2000, pp. 555–558, doi: 10.4028/www.scientific.net/msf.338-342.555.